Phase determination from mostly one-sided interferograms

David G. Johnson, Wesley A. Traub, and Kenneth W. Jucks

Smithsonian Astrophysical Observatory, 60 Garden Street, Cambridge, Massachusetts, 02138

Abstract

We show how to detect and correct for nonlinear phase shifts in a mainly one-sided interferogram of an emission-line source. We simultaneously detect and correct for an out-of-phase emission background from the spectrometer. The method requires two auxiliary spectra, one of a strong continuum source, and one of an emission-line source with little or no continuum.

Key words: Fourier transform spectroscopy, interferometer, phase.

1. Introduction

Phase determination for an ideal interferometer amounts to finding the position of zero path difference (ZPD) for each spectral element in a recorded interferogram. In this case, the interferogram, $F(x')$, of a single unresolved spectral line centered at wavelength $\lambda_0 = 1/\sigma_0$ is given by $F(x') = a\cos 2\pi\sigma_0(x'-x)$, where x is the position of ZPD and x' is the retardation of the retroreflector in the long arm of the interferometer. The instantaneous optical path difference (OPD) is given by $x'-x$. In the ideal case in which an interferogram sample point falls precisely on the peak of the interferogram, we have $x = 0$, but in general $x \neq 0$. The transform of a one-sided interferogram gives

$$\begin{aligned} F(\sigma) &= \frac{1}{L}\int_0^L F(x')\exp(i2\pi\sigma x')\,dx' \\ &= \frac{a\exp(i2\pi\sigma_0 x)}{2}\left[\frac{\sin\alpha}{\alpha} + i\,\frac{(1-\cos\alpha)}{\alpha}\right], \end{aligned} \tag{1}$$

where L is the length of the scan, $\alpha \equiv 2\pi(\sigma-\sigma_0)L$, and we have dropped terms containing $(\sigma+\sigma_0)$. The transform of a mostly one-sided interferogram (in which the integral limits are $-L_1$ to $+L_2$, $L_1 \ll L_2$, and a tapering function is applied between $-L_1$ and $+L_1$ to avoid double counting of the two-sided part of F) is similar, but it differs in details that are not important here. In either case, once we have determined x, we recover the spectrum by taking the real part of $F(\sigma)\exp(-i2\pi\sigma_0 x)$. The transform of a two-sided interferogram (in which the mirror scans from $-L$ to L) for the same unresolved line is simply $a\exp(i2\pi\sigma_0 x)\sin\alpha/2\alpha$.

The phase of transform $F(\sigma)$ in Eq. (1) is given by a slowly varying term ($2\pi\sigma_0 x$), plus a rapidly varying term, $\tan^{-1}[(1-\cos\alpha)/\sin\alpha]$, which is only significant near a spectral line. We have found that, for our interferometer, the slowly varying term is not well modeled by linear function $2\pi\sigma x$. In Sections 3–5 we present a method for detecting and correcting for a small nonlinear phase shift. We simultaneously detect and correct for an out-of-phase emission background from the spectrometer.

Equation (1) illustrates a crucial element of our phase-recovery method, line symmetrizing, which is discussed in Section 4. Phase factor $2\pi\sigma_0 x$ in Eq. (1) is not known a priori but must be estimated. If the estimated phase equals $2\pi\sigma_0 x$, then the real part of Eq. (1) gives a symmetric line, from the $\sin\alpha/\alpha$ term. If the estimated phase is $2\pi\sigma_0 x \pm \pi/2$, then the real part of Eq. (1) gives an antisymmetric line, from the $(1-\cos\alpha)/\alpha$ term. In practice, it is straightforward for us to select the optimum phase factor that symmetrizes the real part of a complex spectral line by multiplying the region around the line by a series of equispaced phase factors and by testing the real part of each result for symmetry.

2. Instrument description

The far-infrared spectrometer (FIRS-2) was designed and built at the Smithsonian Astrophysical Observatory for the purpose of measuring stratospheric emission spectra from balloon and aircraft platforms. The spectrometer produces mostly one-sided interferograms, which must be transformed and accurately phase corrected before the spectra can be used to retrieve constituent profiles. The FIRS-2 and data-reduction procedure are described in detail elsewhere;[1,2] our phase-recovery method is summarized elsewhere[2] but is fully discussed here. A brief description of the instrument as configured for balloon flights follows.

The flight instrument consists of a limb-scanning telescope, the interferometer, detectors, and associated control electronics. The telescope is a small off-axis reflector that is pointed in elevation relative to a single-axis stabilized platform.[3,4] The interferometer uses hollow corner-cube retroreflectors and a 11-μm uncoated Mylar beam splitter, and it scans over OPD's from $-L_1$ to $+L_2$, where $L_1 = 1.2$ cm and $L_2 = 120$ cm. We use two liquid-helium-cooled detectors, a gallium-doped germanium photoconductor for the band from 75 to 220 cm^{-1} and a copper-doped germanium photoconductor for the band from 330 to 700 cm^{-1}. The field of view is defined by field stops near the detectors.

During a balloon flight we record interferograms for a sequence of elevation angles, repeating the sequence throughout the flight. We first observe an ambient-temperature blackbody source at an elevation angle of 90°, followed by a space

view at 30°, and then we observe the limb at elevation angles of 0.0°, −2.3°, −3.0°, −3.6°, −4.2°, and −4.6°. A complete sequence takes approximately 2700 s. We show small segments of sample flight spectra for 90°, 30°, and −4.17° in Fig. 1, recorded at a balloon altitude of 36 km. The spectra have been phase corrected by using the method outlined below, but they have not been calibrated in intensity or wave number. Note the presence of a substantial out-of-phase (negative) instrumental background in the 30° spectrum. The phase-recovery method discussed here is not affected by this background, which is later detected and corrected for.

3. Model description

We assume that the measured blackbody spectrum, $M_{90}(\sigma)$, can be modeled as

$$M_{90}(\sigma) = \{B(\sigma) + E(\sigma)\exp[i\phi(\sigma)]\} \times \exp\{i[2\pi\sigma x_{90} + \varepsilon(\sigma)]\}, \quad (2)$$

where $B(\sigma)$ is the product of the instrumental response function and a blackbody spectrum, $E(\sigma)\exp[i\phi(\sigma)]$ is the complex background spectrum,[5] x_{90} is the position of ZPD in the blackbody interferogram, and $\varepsilon(\sigma)$ is the nonlinear phase shift.

Similarly, we model the measured space and limb spectra as

$$M_{30}(\sigma) = \{S_{30}(\sigma) + E(\sigma)\exp[i\phi(\sigma)]\} \times \exp\{i[2\pi\sigma x_{30} + \varepsilon(\sigma)]\}, \quad (3)$$

$$M_{\theta}(\sigma) = \{S_{\theta}(\sigma) + E(\sigma)\exp[i\phi(\sigma)]\} \times \exp\{i[2\pi\sigma x_{\theta} + \varepsilon(\sigma)]\}, \quad (4)$$

where S_{30} and S_{θ} are the phase-corrected space and limb spectra and x_{30} and x_{θ} are the positions of ZPD in the respective interferograms.

In this notation, the $M_{90,30,\theta}(\sigma)$ functions are complex spectra that we obtain by applying a fast Fourier transform to an observed and windowed interferogram, where the window function is typically a weight running linearly from 0 to 1 between $-L_1$ and $+L_1$ and a constant weight of 1 between $+L_1$ and $+L_2$. Also in this notation, the functions on the right-hand sides of Eqs. (2)–(4) [$B(\sigma)$, $S_{30,\theta}(\sigma)$, $E(\sigma)$, $\phi(\sigma)$, $\varepsilon(\sigma)$, and $x_{90,30,\theta}$] are all to be extracted from the $M(\sigma)$ data and therefore include a random noise component. The recovered spectra, B and $S_{30,\theta}$, are phase corrected but must be calibrated by wave number[2] and intensity[2,5] (see also Section 5).

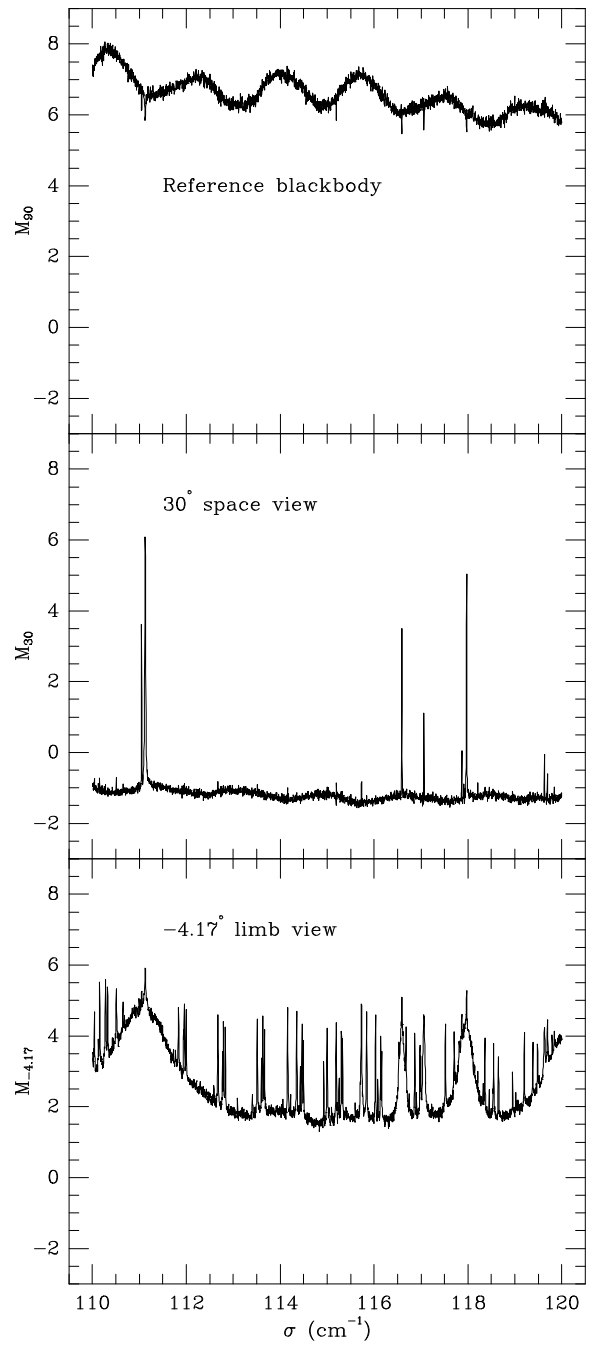

Fig. 1. FIRS-2 spectra recorded at a balloon altitude of 36 km. Vertical scale (arbitrary units) is the same for each graph. The elevation angles are indicated; at 90° the telescope views a reference blackbody.

From typical balloon altitudes, space spectrum S_{30} consists of a few narrow emission lines with no continuum emission, limb spectra S_θ contain many lines superposed on a substantial continuum, and blackbody spectrum B consists of continuum alone. We assume that the background spectrum, $E(\sigma)\exp[i\phi(\sigma)]$, is constant for the duration of an observation sequence, and that $\varepsilon(\sigma)$ is constant for any given balloon flight. As we show in Section 4, ε does indeed seem to be constant with respect to time.

4. Estimate of nonlinear phase

As we mentioned in Section 2, each interferogram consists of a low-resolution two-sided part (maximum OPD range of $\pm L_1 = \pm 1.2$ cm) and a high-resolution one-sided part (maximum OPD of $L_2 = +120$ cm). Both the low- and high-resolution interferograms are used in the steps that follow; we use m to represent the transform of the low-resolution two-sided interferogram, and M to represent the high-resolution transform. The basic procedure is for us to estimate x_{30} by using high-resolution spectrum M_{30}, estimate x_{90} by using low-resolution spectrum m_{90}, and then estimate $\varepsilon(\sigma)$ by calculating the phase of the difference $m_{90} - m_{30}$ at low resolution. In the following step-by-step procedure we have omitted some details (tapering functions used for low- and high-resolution transforms, zero padding, and the like) for brevity and clarity; further details regarding our routine implementation of the fast Fourier transform are presented in Ref. 2.

Our method differs from one previously described in Ref. 6 in that it requires two auxiliary spectra but works for almost totally one-sided interferograms. The radiometric calibration method described in Ref. 5 calibrates and phase-corrects spectra in a single step, but it requires saving the complex transforms of hot and cold calibration spectra. Neither method is capable of determining phase factor $2\pi\sigma_0 x$ when the two-sided transform is dominated by the complex background, $E(\sigma)$.

Step 1. To begin, we examine the nominal (theoretical or experimental) spectra to be analyzed and select a large number (40–60) of spectral lines that we anticipate should be intrinsically symmetric with respect to reflection about their central wave numbers. For each line in this group, estimate a value of x_{30} by symmetrizing the line in the full-resolution 30° spectrum. As we can see by examining Eq. (1), we can determine the phase (modulo π) for a spectral line at σ_i by finding phase β_i for which $M_{30}\exp(-i\beta_i)$ is symmetric near the line center. We calculate $\bar{x}_{30}$ by fitting function $\beta(\sigma) = 2\pi\sigma\bar{x}_{30}$ to the derived set of (σ_i, β_i) values. The residuals from the fit are a combination of the error in estimating β_i and the nonlinear phase term $\varepsilon(\sigma_i)$. In practice, the uncertainty in β_i is too large to get a good estimate of $\varepsilon(\sigma_i)$ from the residuals.

Step 2. Calculate m'_{30}, the low-resolution space spectrum with the linear phase removed:

$$m_{30}(\sigma)\exp(-i2\pi\sigma\bar{x}_{30}) = [S_{30} + E\exp(i\phi)]\exp(i\varepsilon), \tag{5}$$

$$\equiv m'_{30}. \tag{6}$$

Step 3. Estimate x_{90} by calculating the phase from the transform of the short two-sided part of the blackbody interferogram. We calculate phase β_i at each point in regions where $B(\sigma) \gg E(\sigma)$, and again we fit a linear function to the set of (σ_i, β_i) to derive $\bar{x}_{90}$. The residuals from this fit would give a good estimate of $\varepsilon(\sigma)$, but only in regions where the background is small.

Step 4. Calculate m'_{90}, the blackbody spectrum with the linear phase removed:

$$m_{90}(\sigma)\exp(-i2\pi\sigma\bar{x}_{90}) = [B + E\exp(i\phi)]\exp(i\varepsilon), \tag{7}$$

$$\equiv m'_{90}. \tag{8}$$

Step 5. Calculate the nonlinear phase, $\varepsilon(\sigma)$:

$$m'_{90} - m'_{30} = [B + E\exp(i\phi)]\exp(i\varepsilon) - [S_{30} + E\exp(i\phi)]\exp(i\varepsilon), \tag{9}$$

$$= (B - S_{30})\exp(i\varepsilon), \tag{10}$$

$$\varepsilon(\sigma) = \tan^{-1}\left[\frac{\Im(m'_{90} - m'_{30})}{\Re(m'_{90} - m'_{30})}\right]. \tag{11}$$

Step 6. Repeat the process for a number of pairs of M_{90} and M_{30}, average the results, and smooth the average to produce the final estimated nonlinear phase term, $\bar{\varepsilon}(\sigma)$.

In Fig. 2 we show $\bar{\varepsilon}(\sigma)$ for two sets of measurements made several years apart that use different beam splitters. The estimated phase is unreliable near minima in the beam-splitter efficiency function because in these regions $B \ll E$ and difference $m'_{90} - m'_{30}$ is dominated by noise. Outside these regions the two phase estimates are in excellent agreement, indicating that $\varepsilon(\sigma)$ is constant in time and independent of beam-splitter thickness. A discussion of the possible physical origin of the nonlinear term, $\varepsilon(\sigma)$, is found in Ref. 5.

5. Background estimate and normalization

Step 7. Estimate the background, $E\exp(i\phi)$, by clipping lines from the high-resolution phase-corrected spectrum,

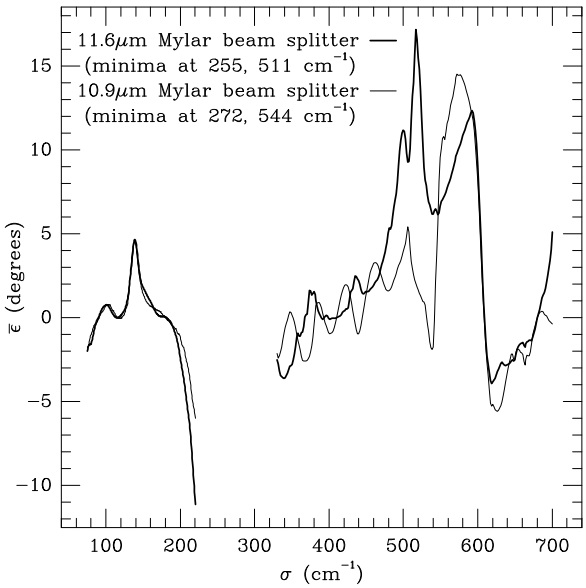

Fig. 2. Nonlinear phase term $\bar{\varepsilon}$ estimated for two different Mylar beam splitters. The data from 75 to 220 cm^{-1} are from the far-infrared detector, and data from 330 to 700 cm^{-1} are from the midinfrared detector.

$M'_{30}\exp(-i\bar{\varepsilon})$, and smoothing the result, as follows. First remove nonlinear phase $\bar{\varepsilon}(\sigma)$ from the high-resolution space spectrum, M'_{30}:

$$M'_{30}\exp(-i\bar{\varepsilon}) = \{[S_{30} + E\exp(i\phi)]\exp(i\varepsilon)\} \times \exp(-i\bar{\varepsilon}), \quad (12)$$

$$= S_{30} + E\exp(i\phi). \quad (13)$$

Then effectively subtract S_{30} by clipping the sharp spectral lines from the result:

$$M'_{30}\exp(-i\bar{\varepsilon}) - S_{30} = E\exp(i\phi), \quad (14)$$

$$\equiv M''_{30}. \quad (15)$$

Clipping lines is equivalent to subtracting S_{30} because the continuum emission in the space view is negligible. The clipping is accomplished numerically when each apparent sharp spectral line (above a preset noise threshold) is replaced with a straight-line segment that bridges the adjacent spectral regions.

Step 8. Calculate the estimated limb spectrum, $S_\theta(\sigma)$, for the remaining elevation angles by estimating $\bar{x}_\theta$ as for $\bar{x}_{30}$, phase correcting, and subtracting the background as follows:

$$M_\theta\exp(-i\bar{\varepsilon})\exp(-i2\pi\sigma\bar{x}_\theta) - M''_{30} = [S_\theta + E\exp(i\phi)]\exp[i(2\pi\sigma x_\theta + \varepsilon)] \times \exp(-i\bar{\varepsilon})\exp(-i2\pi\sigma\bar{x}_\theta) - E\exp(i\phi), \quad (16)$$

$$= S_\theta(\sigma). \quad (17)$$

Step 9. Calculate the observed response, $B(\sigma)$, to the blackbody source:

$$M'_{90}\exp(-i\bar{\varepsilon}) - M''_{30} = B(\sigma). \quad (18)$$

Step 10. Calculate the intensity-calibrated limb spectra, $S_\theta^{\rm cal}(\sigma)$, from the derived $S_\theta(\sigma)$ and $B(\sigma)$:

$$S_\theta^{\rm cal}(\sigma) = \frac{S_\theta(\sigma)P(T_{bb},\sigma)}{B(\sigma)P(277\ {\rm K},\sigma)}, \quad (19)$$

where $P(T,\sigma)$ is the Planck function, T_{bb} is the measured temperature of the reference blackbody source, and 277 K is a standard reference temperature, chosen for convention in our data-analysis procedure. Resulting spectra $S_\theta^{\rm cal}(\sigma)$ are dimensionless and independent of the instrument spectral response, which is convenient for plotting and visualization. We can easily recover spectra in physical units (erg cm^{-2} s^{-1} st^{-1}) by multiplying by $P(277\ {\rm K},\sigma)$.

6. Results

We judge the success or failure of the phase determination by comparing measured and calculated emission-line spectra and looking for systematic differences. As we mentioned in Section 4, the scatter in estimated phase β_i is too large for us to be able to judge the effect of the nonlinear phase term on single spectra. In coadded spectra, however, the improvement is considerable in regions where $\varepsilon(\sigma)$ is large, particularly in the region 560–610 cm^{-1}, where the nonlinear term is as large as 15°. This region is used for fitting CO_2 and N_2O in FIRS-2 spectra, and correcting for the nonlinear phase term eliminates a systematic difference between observed and calculated line shapes in this region. Spectra that have been phase corrected by the use of the method outlined in this paper have emission-line profiles that are visibly more symmetric than results from the assumption of a linear phase function, as shown in Fig. 3, and they are a much better match to calculated spectra. Failing to correct for the nonlinear phase term not only results in a shift in the line position but also produces highly asymmetric line wings.

7. Conclusion

We describe a method for phase-correcting and calibrating emission spectra from mostly one-sided interferograms. The method, developed for the FIRS-2, is effective in the presence of an out-of-phase background.

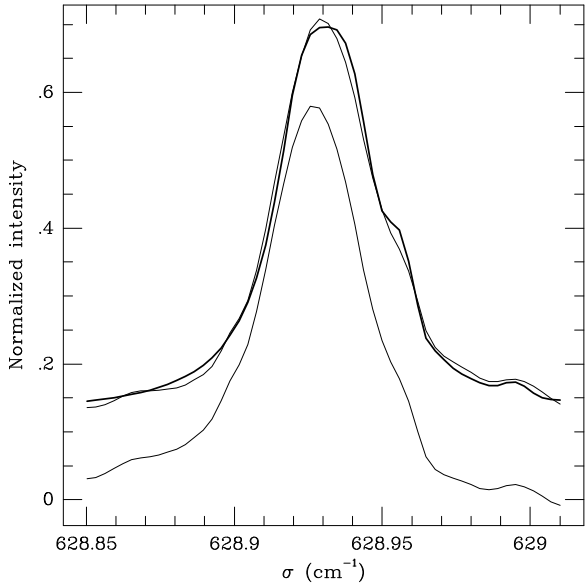

Fig. 3. Portion of a flight spectrum that shows the effect of ignoring the nonlinear phase term, $\bar{\varepsilon}$. The upper curve was produced with the phase-recovery method outlined in this paper; the thick curve indicates a calculated spectrum for the same region. The lower curve shows the result after we assume that $\bar{\varepsilon} = 0$. The baselines for the upper curve and calculated spectrum have been shifted by 0.12 for clarity.

The algorithm is in routine use to reduce FIRS-2 spectra, and it has been used for several years now with good success.

ACKNOWLEDGMENTS

We gratefully acknowledge support from NASA's Upper Atmosphere Research Program in the form of grant NSG 5175.

1. W. A. Traub, K. V. Chance, D. G. Johnson, and K. W. Jucks, “Stratospheric spectroscopy with the far-infrared spectrometer (FIRS-2): Overview and recent results,” Proc. Soc. Photo-Opt. Instrum. Eng. **1491,** 298-307 (1991).
2. D. G. Johnson, K. W. Jucks, W. A. Traub, and K. V. Chance, “Smithsonian stratospheric far-infrared spectrometer and data reduction system,” J. Geophys. Res. **100,** 3091-3106 (1995).
3. L. M. Coyle, G. Aurilio, G. U. Nystrom, J. Bortz, B. G. Nagy, K. V. Chance, and W. A. Traub, “Design of a single-axis platform for balloon-borne remote sensing,” Rev. Sci. Instrum. **57,** 2512-2518 (1986).
4. W. A. Traub, K. V. Chance, and L. M. Coyle, “Performance of a single-axis platform for balloon-borne remote sensing,” Rev. Sci. Instrum. **57,** 2519-2522 (1986).
5. H. E. Revercomb, H. Buijs, H. B. Howell, D. D. LaPorte, W. L. Smith, and L. A. Sromovsky, “Radiometric calibration of IR Fourier transform spectrometers: Solution to a problem with the High-Resolution Interferometer Sounder,” Appl. Opt. **27,** 3210-3218 (1988).
6. R. C. M. Learner, A. P. Thorne, I. Wynne-Jones, J. W. Brault, and M. C. Abrams, “Phase correction of emission line Fourier transform spectra,” J. Opt. Soc. Am. A **12,** 2165-2171 (1995).